Automated high speed 3D imaging of organoid cultures with efficient multi-scale phenotypic quantification

Anne Beghin, Gianluca Grenci, Geetika Sahni, Su Guo, Harini Rajendiran, Tom Delaire, Saburnisha Binte Mohamad Raffi, Damien Blanc, Richard de Mets, Hui Ting Ong, et al.

Automated high speed 3D imaging of organoid cultures with efficient multi-scale phenotypic quantification.

Author(s): Anne Beghin[1,2], Gianluca Grenci[1,3], Geetika Sahini[1], Su Guo[1], Harini Rajendiran[1], Tom Delaire[4], Saburnisha Binte Mohamad Raffi [1], Damien Blanc[5], Richard de Mets[1], Hui Ting Ong[1], Miguel Sambrano[4], Xareni Galindo[4], Anais Monnet[1], Vidhyalakshmi Acharya[1], Victor Racine[5], Florian Levet[4,6], Remi Galland[4], Jean-Baptiste Sibarita[4], Virgile Viasnoff[1,7,8]

Affiliation(s):
[1]Mechanobiology Institute, National University of Singapore, 117411, Singapore.
[2]Immunology Translational Research Programme, Yong Loo Lin School of Medicine, NUS Department of Microbiology & Immunology, NUS
[3]Biomedical Engineering Department, National University of Singapore, 117583, Singapore.
[4]Univ. Bordeaux, CNRS, Interdisciplinary Institute for Neuroscience, IINS, UMR 5297, F-33000 Bordeaux, France
[5]QuantaCell, 33600 Pessac, France
[6]Univ. Bordeaux, CNRS, INSERM, Bordeaux Imaging Center, BIC, UMS 3420, US 4, F-33000 Bordeaux, France
[7]Department of Biological Sciences, National University of Singapore, 117583, Singapore,
[8]IRL 3639 CNRS, 117411 Singapore.

Corresponding authors: Anne Beghin, Virgile Viasnoff

ABSTRACT

Current imaging approaches limit the ability to perform multiscale characterization of 3D organotypic cultures (organoids) in large numbers. Here, we present an automated multiscale 3D imaging platform synergizing high-density organoid cultures with 3D live single objective light-sheet imaging. It is composed of disposable microfabricated organoid culture chips embedding optical components and a custom laser beam steering unit coupled to a commercial inverted microscope. It streamlines organoid culture and high content 3D imaging on a single user-friendly instrument with minimal manipulations and unprecedented throughput of 300 organoids per hour in 3D. Collecting large number of 3D stacks allowed training deep learning-based algorithms to quantify the organoids morphogenetic organizations at multi-scales, ranging from the sub-cellular scale to the whole organoid level. We validated the versatility and robustness of our approach on intestine, hepatic, neuroectoderm organoids and oncospheres.

INTRODUCTION

In organotypic 3D cell cultures, referred hereafter as organoids, stem cells differentiate and self-organize into spatial structures that share strong morphological and functional similarities with real organs. Organoids offer valuable models to study human biology and development outside of the body[1,2,3]. An increasing number of organoids are being developed

that mimic intestines, liver, brain, kidney, lung, and many other organs[2,4,5]. Their differentiation is directed by a precise sequence of exposure to soluble growth factors and extracellular matrix during their development. However, in marked contrast to organs, the morphologies of organoids could be quite heterogeneous. In organs, phenotypic alterations can be used as a proxy to diagnose a diseased state. In contrast, organoids differentiate in minimally reproducible micro-environments resulting in a large variability of their development path and morphology at the individual organoid level. Characterizing and controlling such a diversity results in several technological roadblocks[6,7]. Fast, automated, and multiscale imaging is one of them. In a recent study[8] quantitative imaging of intestine organoid shape coupled to the assessment of a few genetic markers allowed defining the organoids phenotypic development landscapes. The different organization paths that the organoids spontaneously adopted were quantified and causally linked to the biological programs orchestrating the spatial induction of different cell fates. However, such studies, like also in Renner et al. [9] , still required a methodological and technological 'tour-de-force' [10] using a multi-well plate for organoid growth, and commercially available high content imaging techniques performed on fixed organoids at specific time point during their growth. Arguably, the ability to relate the diversity of genomic expression in organoids with their phenotypic behaviour is a major step to guide the establishment of their culture conditions as well as to provide a system biology view of developmental pathways. Hence, it exists a real demand for the development of dedicated high content organoid 3D imaging methods to characterize organoid at sub-cellular, multi-cellular, and whole organoid scales both in 3D [11] and during their growth[11,12].

Optical sectioning fluorescent microscopy techniques, such as confocal or multiphoton laser scanning, hardly fit the needs of both high throughput and low photobleaching/phototoxicity for 3D/live imaging. Commercially available high content screening platforms (e.g. PerkinElmer's Opera or Molecular Devices' ImageXpress), are usually well adapted for 2D cell cultures. However, they generally offer low speed, penetration depth, high bleaching, and image analysis issues when applied to 3D cultures. Light-sheet fluorescence microscopy (LSFM) is undoubtedly the most appropriate imaging technique to visualize fine cellular details at the whole tissue level, with maximal speed and minimal phototoxicity and photobleaching[13]. LSFM has thus been favored for the study of live organoids, as it allows long-term monitoring in physiological conditions[14]. However, it traditionally involves several objectives, and despite its superior imaging performances, it results in low imaging throughput due to cumbersome sample mounting requirements. Recent studies using dual objective SPIM have tried to engineer solutions to improve the throughput[15] using a liquid handling robot and complex dedicated imaging hardware. However, this solution does not permit long term sterile culture (more than 24 hours), as periodic medium or extracellular matrix exchange is mandatory for organoid development and differentiation. To overcome these important limits, several approaches have been developed to perform LSFM with a single objective. High speed, high content SCAPE[16] was used to obtain ultra-fast images of *in vivo* processes in individual *C. elegans* and *Zebra fish.* Alleviating the multi-objective constraint, other approaches proved capable to image multiple samples. Epi-illumination SPIM (ssOPM) enabled parallel 3D volume acquisition of single cell down to the single molecule level in 96 well plates[17]. It also allowed the imaging of living oncospheres in 3D seeded in agarose to detect glucose uptake[18] but only during a short period

of time (3 hours). Moreover, the random positioning of the spheroids in the agarose limited the study to 42 oncospheres.

It follows that existing technological solutions still offer important room for improvement for 3D high content imaging of live and fixed organoids.

In this context, we developed a versatile high content (i.e multi-scale) imaging platform to streamline organoid culture (from isolated hESC, hIPSC or primary cells to 3D multicellular differentiated organoids) with fast non-invasive 3D imaging. It integrates a new generation of miniaturized 3D cell culture device, called the JeWell chip. They comprise thousands of well-arrayed microwells (JeWells) flanked with 45° mirrors to enable large scale single objective light-sheet microscopy (soSPIM)[19]. Compatible with standard commercial inverted microscope after simple addition of a beam steering unit and a dedicated control software, our system performs 3D imaging of up to 300 organoids in an hour with subcellular resolution and minimum photobleaching. We tested it on various organoid models (hepatocytes, neuroectoderm, intestinal) and 3D cell cultures (hESC, HCT116). We leverage the large throughput of the approach to train several public-domain convolutional neural networks to extract relevant biological features at different scales, ranging from the sub-cellular, cellular and multi-cellular scales, up to the whole organoid. We demonstrate how the technique enables correlative imaging at different magnifications and resolutions, or between live development and endpoint imaging of immunolabeled proteins or gene expression profile of organoids.

RESULTS

Streamlining high density organoid culture with automated high content 3D imaging.

Figure 1 illustrates the dedicated disposable microfabricated JeWell chips used to create high density arrays of organotypic cell aggregates for automated high content 3D soSPIM imaging. JeWells are truncated pyramidal shaped micro-cavities moulded in a photocurable resin (NOA73) with 45° gold coated faces **(Figure 1a)**. The detailed protocol (Online Methods) for their microfabrication is illustrated in the **Supplementary Figure 1**. The JeWell microcavities are arrayed at a typical surface density of *150* JeWells/15 mm^2, depending on individual JeWell sizes, corresponding to the equivalent of 96 organoids in a single well of a standard 384 well plate. This ensures an optimal scanning distance between JeWells for high-speed 3D soSPIM imaging. We devised the JeWell chips with various sizes and shapes in the format of single Petri dishes, 6 well format or 96 well plates (**Supplementary Figure 1-2**). A Lipidure® coating was used as an enduring antifouling treatment to prevent any adhesion of the cell culture on the JeWell chips over months allowing long term 3D cell cultures (detailed protocols provided in **Online Methods**). Single cells or small cell aggregates were seeded homogeneously over the chips (**Figure 1b)**. Buoyancy mismatch leads cells to sink at the bottom of the JeWells (**Figure 1b**). The JeWell chips compatibility with phase contrast imaging allows monitoring the formation of cell aggregates and assess their homogeneity. Rapidly after the seeding phase, it enabled counting the number of cells per individual JeWell as a reference point (**Online Methods)**. **Supplementary Figure 3** illustrates the reproducibility of the seeding procedure, demonstrating how the initial cell concentration and the seeding time allows to precisely control the number of cells per JeWell (eg: $0.5x10^6$ cells/ml for 10 min leads

to 96 $\pm$ 10 SD cells/JeWell (N=100 wells)). We then monitored by phase contrast microcopy the projected area of the compact aggregates forming within the first few hours post-seeding (**Online Methods**). We observed a batch-to-batch variability of 10% (3 batches) and 25 % dispersion of inter-JeWells aggregate sizes (N=100 organoids). Phase contrast imaging was also used over a prolonged period of time (up to 30 days) during the differentiation protocol to monitor and demonstrate a fairly homogeneous proliferation rate of the organoids (**Supplementary Figure 3**). This procedure proved to be robust for all the tested cell types. In the rest of the paper, cells are subsequently differentiated and grown in the JeWell cavities, except when specified otherwise.

We then positioned the chips on a commercial inverted Microscope (Nikon Eclipse) equipped for single-objective Selective Plane Illumination Microscopy (soSPIM) as described in Galland et al.[19] The imaging system is composed of: *i*- interchangeable lenses (20x air (NA=0.75) and 60x WI (NA=1.27) used here but not limited to) (**Figure 1c**) *ii*- a custom laser scanning unit and *iii*- an acquisition module operating inside MetaMorph commercial software. The **Online Methods** and **Supplementary Figure 1** detail the acquisition set-up. In brief, the 45° gold coated micromirrors of the JeWells enable to reflect a laser beam **(Figure 1d)** focused on the sample by the same objective used for imaging. Scanning the laser beam along the mirror axis (y-direction) creates a light-sheet perpendicular to the optical axis of the objective, illuminating a thin section of the sample. The fluorescent signal is then collected through the same and single objective used to create the light-sheet. Translating the laser beam perpendicularly to the mirror (x-direction) translates of the light-sheet along the optical axis of the objective (z-direction). Synchronizing the light-sheet position with the focal plane of the objective ensures optimal 3D optical sectioning. The integration of the optical components inside the chips eliminates the steric and alignment constraints of traditional multi-objective light-sheet microscopes. We devised an automatic acquisition pipeline that integrates *i*- an optional pre-screening step, *ii*- the automated identification and user-assisted selection of the JeWells containing organoids to image, *iii*- the precise automatic positioning of the light-sheet on the JeWell mirrors (**Online Methods** and **Supplementary Figure 4**). This allows to rapidly setup the sequential 3D multi-colour imaging of hundreds of organoids in a single acquisition workflow, with minimal user interaction. This approach builds on our previous work[19] devised for single molecule imaging in 3D using single objective SPIM (soSPIM). With a 60x 1.27 NA objective, we could acquire images with a lateral resolution of around 300 nm. The light-sheet thickness could be manually adjusted between 2 µm to 3.7 µm for a length of 12 µm to 60 µm respectively using a 60x magnification. A light-sheet of 5.7 µm thick for 135 µm long was obtained with a 20x magnification objective. We took benefit of the JeWells as proxies for automatic alignment and calibration of the light-sheet as well as for drift correction (**Supplementary Figure 4**).

This new integrated imaging platform provided a very efficient way to perform long term automatic 3D imaging of various organoids with unprecedented throughput and limited manipulation. **Figure 1e** illustrates a collection of 96 neuroectoderm organoids differentiated from hESCs, fixed at day 8 and immunostained for Nuclei (405nm), Sox2 (488nm) and N-cadherin (647nm) (**Material and Methods**). Setting-up the entire screening parameters and selection of 96 organoids took around 10 min using a 60x WI 1.27NA objective, including the

high-resolution pre-screening of the JeWell chip. Each 3D stacks of immunostained fixed organoids took about 7 sec per wavelength for 70 optical sections using one side light-sheet illumination. The time between two adjacent JeWell acquisitions was 1.5 sec and the light-sheet repositioning accuracy below 50 nm. It took 1h to acquire 96 organoids with 70 z-planes for 3 wavelengths, representing a total of 173GB of raw data. The sectioning and the quality of the images shown in **Figure 1e** insert illustrates the level of sub-cellular details that can be resolved.

Compatibility with various 3D cell culture types.

We then demonstrated the robustness and the versatility of the approach by culturing and imaging a wide variety of organotypic systems thanks to JeWell cavities that matched the final size and shape of the targeted organoids (**Figure 2a**, **Supplementary Figure 2**). We grew a variety of primary cells, embryonic cells, cancer cells in the JeWell chips according to individual protocols described in **Online Methods**.

Figure 2b shows that aggregates of primary rat hepatocytes developed secreting bile canaliculi (2 µm diameter intercellular lumens). Using MRP2 (bile transporter) as a marker of functional canaliculi, we could reconstitute the canalicular network in 3D (**Movie 1**).

Figure 2c exemplifies the culture of neuroectoderm organoids successfully differentiated from human embryonic stem cells (hESCs). They displayed the characteristic transcription factors for early ectoderms and developed *bona fide* rosette multicellular organisation. 3D soSPIM imaging with a 60x 1.27NA WI objective allowed to resolve single actin protrusions within the rosette core with a lateral resolution of about 300 nm.

Figure 2d exemplifies the culture of HCT116 human colon carcinoma cells aggregated in oncospheres that displayed a clear hypoxic core when cultured under low oxygen conditions. Staining with Ki67 revealed the proliferation stages of the cells inside each oncosphere.

Figure 2e displays the images of human stem cells cultured in Matrigel for 7 days within alginate micro-capsules (TreeFrog Therapeutics technology), removed from their capsules, seeded and imaged in large number in JeWell cavities with large top opening (270 µm). It revealed the multilayer cyst that formed in each alginate capsule.

Figure 2f, finally, shows early (8 days) and late (20 days) intestinal organoids cultured and imaged in elongated JeWell grooves. At day 8, the organoids displayed sparse regions of CDX2 positive cells. At day 20, CDX2 was ubiquitously expressed with a strong Villin signal lining the apical pole of the elongated lumen within each of the organoids. The format of the elongated JeWell grooves provided a scaffold to orient the organoids' growth.

Altogether, we successfully grew and imaged functional organoids and oncospheres in the JeWell chips. It illustrates the great potential of our approach to collect large collections of high resolution 3D images of organoids that are either directly grown inside the JeWell chips, or produced outside and seeded after. The image quality is in agreement with state-of-the-art single side Gaussian light-sheet illumination expectation.

Automatic quantification of cell localization and proliferation states

Single side illumination scheme proved to be an excellent compromise between acquisition speed, phototoxicity, and image quality to perform reliable automated quantitative analysis.

The simple and fast 3D acquisition of a large number of organoids, makes the system particularly suited to implement deep learning-based quantitative analysis. As an illustration, we first analysed HCT116 aggregates (human colon cells) grown in the JeWell chips. The aggregates originated from 80 cells ±20, which reached different sizes after 10 days proliferation. We then fixed and stained them for Nuclei (DAPI) and Ki67 as a marker for chromosome contours, and acquired 3D stacks with the soSPIM using the high content 3D imaging protocol described above. We trained the convolutional neural network (CNN) StarDist over 471 planes (5274 nuclei) manually annotated in 3D from the DAPI images (**Online Methods**). The quality of the 3D segmentation of the nuclei (**Online Methods)** is exemplified in **Figure 3a**. We manually compared the ground truths to the predictions in 3D on 10 organoids, assessing a detection accuracy superior to 85% (**Movie 2**). Importantly the detection accuracy was equivalent on both sides of the oncosphere, demonstrating that the Stardis CNN was insensitive to the inhomogeneities originating from the single sided Gaussian illumination (**Supplementary Figure 5**).

We then used the Ki67 channel to detect and classify proliferating cells[20]. We used the Yolov5 convolutional neural network to detect and classify dividing cells (**Online methods**) into three proliferation phases: G1/S/G2 (large dense clusters of Ki67), Mitosis (condensed chromatide marked by Ki67) and Early G1 (Nuclei with scattered Ki67 aggregates), with an accuracy of 90% (**Figure 3b, Movie 3**). G0 cells were Ki67 negative. We found that the number of nuclei scaled logically with the volume of the organoids (**Figure 3c**). However, the fraction of Ki67 positive nuclei decreased with the total number of nuclei per organoids, indicative of a reduced proliferation rate with the organoids size. Further analysis showed that cells were arrested more specifically in G0 phase as the organoids grew. Indeed, amongst the proliferative cells, the proportion of early G1 and Mitosis was insensitive to the organoid volume, indicating that the division cycle time was independent of the organoid size with no arrest at any other proliferation check point.

3D multiscale analysis of organoid morphologies

Beyond nuclei segmentation and proliferation analysis, we further demonstrated that our method enables a multiscale analysis of the organoids morphology through the analysis of neuroectoderm organoids[21] at day 8. We used YoloV5 CNN to localize in 3D mitotic and cell death events directly from the DAPI images. Using 28 annotated organoids, we reached an accuracy of 89% (4% false positive, 7% false negative, benchmarked on 20 test organoids by a trained human). **Figure 4a** shows the 3D organization of the mitotic and cell death events. They appeared homogeneously distributed within the organoid volume, as expected for healthy proliferating organoids. This spatial homogeneity was confirmed by the equal average density of mitotic and cell death computed in 3D regions of interest located in the central *vs* peripheral regions of the organoids (**Online Methods**). It demonstrates that the classification of proliferation events can be performed on different types of organoids.

We then characterized the spatial distribution of cells expressing differentiation markers. Neuroectoderm organoids organized locally in multicellular rosette structures (**Figure 4b**) characterized by layers of aligned cells surrounding a central streak that develops into a lumen[22,23,24,25] . We used the 3D StarDist CNN to segment individual nuclei from the DAPI

channel, and computed the average expression of Sox2 in each segmented nucleus. The distribution of expression levels proved to be bimodal. We thus binarized the distribution between Sox2 positive and Sox2 negative cells by setting a threshold value at the bimodal intersection point (680 au). It allowed us to reconstitute a 3D map of the Sox2 expressing cells in each organoid (**Figure 4b**), clearly revealing the rosette organisation with Sox2 positive cells surrounding the central streak. We then endeavoured to segment the rosettes based on the actin organization, an ubiquitous marker for any cell type that could be used generically in live cell imaging. In that perspective, we trained a U-Net CNN (**Online Methods**) to segment the rosettes in 3D (**Figure 4c, Movies 4-5**). It enabled to extract the number of rosettes per organoids as well as their morphological features for further classification (**Supplementary Table 3**, **Supplementary Figure 7**) (N=415 streaks longer than two cells (20µm)).

Finally, we assessed the neuroectoderm variability of the organoid whole shapes using the shape recognition CNN DenseNet121[26] (**Online Methods**) to classify automatically the organoids in two morpho-classes: bean shaped (B-shaped) or spherical shape (O-shaped) (**Figure 4e**) with 99 % accuracy (**Supplementary Figure 6b**). Interestingly, B-shape organoids systematically displayed fewer nuclei and internal rosettes than O-shape ones.

Altogether, we demonstrated that our integrated densely arrayed culturing JeWell chips combined with our high content 3D imaging platform allows training efficiently different CNN to quantitatively assess neuroectoderm organoids at several scales, ranging from the single cell level, up to the whole organoid level.

Multi-magnification capabilities and image analysis allow efficient extraction of rare events

We then demonstrated that the organoids can also be imaged at different magnifications to facilitate the localization of rare cellular clusters composed of a few cells expressing specific markers. We used intestinal organoids that have been grown and differentiated for 8 days (early stage) (**Figure 5**). We fixed and stained them for nuclei (DAPI), actin, CDX2 (a major regulator of intestine-specific genes) and E-cadherin (E-cad). As expected, at these early stages of differentiation, only a fraction of the cells was CDX2 positive. We leveraged on the arrayed organization of the organoids grown in JeWell chips to perform correlative multi-magnification 3D imaging. First, we rapidly scanned 100 organoids in 3D (10 min for 100 organoids) at 20x magnification (air objective, 10 Z plans, 7 microns Z-steps) only for two channels (CDX2 and actin) (**Figure 5a**). The CDX2 channel was then automatically analyzed and we identified the CDX2 positive organoids ($CDX2^+$) as representing 20% of the whole library. We next performed a second scanning of the $CDX2^+$ organoids for the 2 other channels (E-cad and DAPI) to screen the E-cad expression profile at this early stage, still at low magnification (20x) but with higher axial sampling (**Figure 5b**, 50 plans, 1 micron z-steps, 10 min for 20 organoids). An automated segmentation (**Online Methods**) within the E-cad channel (**Figure 5b**) allowed identifying E-cad expressing cells clusters ($Ecad^+$) present in 25% of the $CDX2^+$ organoids (5% of the whole library of 100 organoids). Finally, a third round of 3D acquisitions at high resolution using a 60x magnification (WI 1.27NA) objective was performed to image exclusively the regions with $E\text{-}cad^+$ cells (4 channels, 50 Z plans, 1 micron z-steps, **Figure 5d**). This high-resolution 3D imaging enabled to reconstruct in 3D the $E\text{-}cad^+$ junctions of CDX2 positive cells, which was not possible at 20x magnification. **Figure 5e** displays one

representative example of 3D reconstruction of E-cad$^+$ cellular cluster where one central cell was surrounded and linked to 4 cells (only five E-Cad$^+$ cells among thousands constituting one single organoid). These 5 cells, localized at the border of the lumen, showed also a very high level of CDX2 compared to the adjacent cells, confirming the link between CDX2 and E-cad expression profiles. Altogether, the acquisition and the analysis took less than 1h. Finding rare cellular clusters within the organoids population was greatly facilitated by the capability of multi-magnification imaging of the soSPIM imaging system.

Live imaging modalities

We finally demonstrated that our approach performs correlative imaging between the morphology of live developing organoids and the end-point analysis of their transcription profiles. We followed in live the 3D development of neuroectoderm organoids. We first stained the intercellular clefts in the organoids (**Figure 6a**) with extracellular dyes (Calcein, AlexaFluor 647). **Supplementary Figure 8** demonstrates that the dyes infiltrated within 15 minutes the entire organoid intercellular volume without effect of the JeWell cavities. It allowed us to monitor in 3D cellular movements during the development of rosettes and streaks (**Movie 6**). To establish the maturation stage of the cells around the rosettes, we fixed the organoids at day 7 and stained them for Sox2 (early development marker) and Pax6 (later development marker). The quality of the repositioning method of individual JeWell enabled to overlap the last images of the live sequence with the immunostained images of the same organoid (**Figure 6b**) by a simple registration in z. It revealed the presence of Pax6 in some rosettes and Sox2 in others. We then used the 3D time lapse to back track the rosette formation process (**Figure 6a**), which revealed that the Sox2$^+$/Pax6$^+$ rosettes (white arrow) appeared 3 days before the Sox2$^+$/*Pax6* $^-$ rosettes. However, immunostaining only provided access to the spatial distribution of a limited number of transcription factors or protein of interests.

To identify the expression level of a higher number of expression factors and proteins of interest, we thus performed RTqPCR on libraries of organoids after imaging. We first tracked the development of neuroectoderm organoids using stem cells expressing life-act GFP and Histone 2B-mCherry[27] (**Movie 7**). We monitored 25 organoids, capturing one z-stack of 70 optical planes every 15 minutes for 8 days, representing a total of 500 3D image stacks per organoid acquired in 125h (**Online Methods**). During these 8 days, we did not notice any obvious effect of photodamaging as mitosis and proliferation continued and no cluster of death cells were observed. Furthermore, at day 8, we did not notice any differences in the organoids size or shape of cellular patterns between the imaged *vs* non-imaged organoids in the JeWell chips. Backtracking the rosettes from day 8, we could follow the time course of the first development steps based on local cell arrangements (**Figure 6c**, **Movie 8**). It revealed that rosette-like structures started to appear in the organoids after 4 to 5 days (consistently with **Figure 6a**). We then collected the organoids alive by peeling-off the JeWell membrane from the glass slide with a sterilized tweezer (**Figure 6c**), and subsequently performed RTqPCR on eleven specific markers (**Online Methods**). Results in **Figure 6c** unambiguously demonstrated the differentiation into neuroectoderm lineage after 8 days of culture in the JeWells as compared to day 2 (undifferentiated stem cell aggregates), characterized by a 10-

fold reduction in Ecad and NANOG, and 500-fold increase in Pax6 for example. This demonstrates that organoids cultured in JeWell chips can be collected for further omics analysis or also be re-seeded in other devices or even injected *in vivo* as the sterility and viability has been conserved.

DISCUSSION

Our automatized high content 3D imaging platform streamlines high-density organoid culture with light-sheet-based 3D fluorescence microscopy. It enables monitoring hundreds of live or fixed organoids in 3D, with an acquisition rate of about 300 organoids per hour, without the need for complex and time-consuming sample manipulation between culturing vessels and imaging supports. It is a versatile platform allowing investigating diverse types of biological systems thanks to the new JeWell culturing device, which dimensions can be scaled according to the expected size and shape of the organoids. In the variety of cells we cultured, we did not see any specific impact of the JeWells on the organoid growth. Organoids can also be grown outside, in dedicated culturing devices, and deposited later inside JeWells for 3D imaging. Our approach leverages on the soSPIM technique developed earlier[19] to perform in depth 3D single molecule localization microscopy in isolated cells. We redesigned the beam steering unit and the acquisition workflow to allow, in combination with the JeWell device, a fully automated high content 3D live imaging of a large number of cell aggregates. It can be easily mounted on any standard inverted microscope, making multi-modal correlative imaging straightforward. We demonstrated that its high-speed acquisition capacity fulfills the requirements of advanced deep learning analysis tools, which require large training data dataset, and provided examples of multiscale quantitative analysis of organoid development. While we performed all the analysis off-line, after the acquisition, the high-speed of the prediction algorithms once trained, will likely allow real time predictive analysis of the organoids while they develop, opening new applications for drug screening and regenerative medicine.

All the soSPIM images we presented were intentionally raw data, with single-side illumination. Their quality proved a good compromise between speed, image quality and processing time. The native quality of our imaging platform was good enough to extract cellular details with good accuracy. However, there are several ways to improve the quality of the images. Multi-side illumination, up to 4, is obviously possible using the different mirrors composing the JeWell cavities. But it comes with a cost of instrumentation complexity, imaging time, photobleaching and image processing time, and should thus be used only if necessary. Line confocal and structured illumination for contrast and sectioning enhancement could also be implemented like for any other traditional SPIM, at not instrumental cost. A significant advantage of our technology over most existing light-sheet approaches, including single-objective ones, is its simplicity to change the objective lens to probe various types of 3D cultures with optimal spatial resolution and field of view, and perform multimodal imaging. Changing magnification also alleviates the requirement of soSPIM to fit both the mirror and the samples within the field of view of the objective. Therefore, with a 60x magnification it is limited to 200 μm width organoids, and with a 20x magnification to 600 μm width organoids. This is not really an issue since most reported organoids are within this size

range: cancer pancreatic[28]: 100 μm, intestinal[29]: 50-200 μm, gastruloids[30]: 100 μm diameter and 400 μm length, liver[31]: 300 μm, micro kidney[32]: 150-200 μm, cancer spheroids[33]: 250-750 μm

A natural future extension of our method is to provide high content screening capacities to allow multi-condition testing in a single workflow. As a proof of concept, we developed a prototype of a 96 well plate integrating arrays of 96 JeWells in each compartment (**Supplementary Figure 1**). Even with the demonstrated unprecedented acquisition speed, imaging the potential 9,216 organoids in 3D with 70 optical planes would take 0.6 TB (resp 1.7 TB) and 1.3 day (resp 4 days) of imaging for a single color (resp 3 colors). The typical analysis time we measured per organoid for the longest convolutional neural network we used is 40 sec per organoids on a standard workstation. Therefore, we estimate that the analysis of the full 96 well plate could be done in 4 days. It could hence be performed almost in parallel as the organoids are acquired. This demonstrates that the imaging scheme we describe here is a good candidate to develop a functional high content screening platform dedicated to organoids.

Our high content organoid 3D imaging approach provides a unique alternative to existing high content screening techniques, offering unsurpassed culturing and imaging throughput, opening new perspectives in the field of organoid research.

DATA AND MATERIAL AVAILABILITY

The raw images of the organoids acquired in this study as well as the training datasets for the convolutional neural networks will be available upon request. We will provide free access to JeWell chips for testing based on Material Transfer Agreement.

CONFLICT OF INTEREST.

The authors declare no conflict of interests.

ACKNOWLEDGMENTS

VV acknowledges the support of NRF investigator NRF-NRFI2018-07, MOE Tier 3 MOE2016-T3-1-005 , MBI seed funding and ANR ADGastrulo. JBS and RG are supported by the Labex BRAIN, Idex Bordeaux, ANR soLIVE (ANR16-CE11-0015) and France BioImaging infrastructure (ANR-10-INSB-04). CNRS PhD fellowship for TD. We thank F. Saltel (BaRiTon lab) for providing the HEP3B-H2B-GFP stable cell-line. We thank P. Cohen, K. Alessandri and A. Leonard (TreeFrog Therapeutics) for providing the encapsulated stem cell cysts. We acknowledge the kind gift of Lifeact/H2D Esc from O. Reiner (Weizmann) and C. Butler for discussions. A.B and GG acknowledges the support from MBI core funding. All authors thank A. Wong and D. Pitta de Araujo for his help editing the manuscript.

ONLINE METHODS

Fabrication methods for the JeWell chips

JeWell pyramidal microwells were produced by casting a textured polymeric thin film using capillarity filling. The textured film was then coated with metal to enhance the reflectivity of the 45° slanted surfaces, flipped, and finally glued to a coverslip to form the final JeWell chips. The detailed fabrication procedure is as follow. First, a silicon primary mold featuring array of

45° truncated pyramidal microwells was made with an optimized process based on the protocol previously published in Galland et al. [19]. The JeWell design required to at least double the previously achieved etch depth, while keeping the same optical finishing. To achieve this, we have revised and modified the overall procedure in order to: (1) Reduce the number of steps required to minimize the introduction of defects during handling of the wafer, (2) Increase the thickness of the oxide layer used to 500 nm, which allowed for longer etching times before the deformation or breaking of the masking layer could introduce defects, and (3) modify the lithographic process and the RIE pattern transfer in order to comply with the higher thickness of the oxide. The fabrication of the JeWell devices required also to modify the fabrication process previously published. First, the silicon primary mold is replicated in PDMS (Supplementary Figure 1a). PDMS Sylgard 184 (Dow Corning) base resin and reticulation agents are mixed in 10:1 ratio and out-gassed (20-30 min in a vacuum jar evacuated to 5-10 mbar). The liquid PDMS is poured on the silicon mold and further out-gassed to ensure filling of the cavities. (vacuum jar at 5-10 mbar for 10 min). After thermal curing (2h at 75 °C on a hot plate) the PDMS mold is peeled-off and cut in 1 x 1 cm^2 pieces. Each 1 x 1 cm^2 cut can be used multiple times to produce JeWell devices.

The PDMS mold features need then to be reproduced onto a glass coverslip. To do so, a PDMS 1x1 cm^2 piece is first flipped face-down on a flat PDMS substrate (Supplementary Figure 1a), then a small amount of liquid UV-curable optical resin (NOA73, Norland Optics, USA) is dropped at one edge of the mold. To be noted that differently from the soSPIM devices, using of an index matched polymer is not required, since the laser sheet is never going to pass through the textured film along its path to reach the organoids inside the pyramidal wells. Thus, cheaper and biocompatible curable resins can be used, such as NOA73. Driven by capillarity, the liquid fills the cavity between the PDMS mold and the flat substrate. Once the whole structured cavity is filled, the NOA is cured by flood exposure to UV light (UV LED KUB2, Kloe France, 365 nm with power density of 25 mW/cm^2, 1 min exposure). Then, the PDMS mold is peeled-off leaving the cured NOA featuring inverted JeWells on the flat PDMS substrate that will have to be flipped 180° around onto a coverslip to end with correctly oriented pyramidal wells. Excess material is trimmed on all 4 edges and a film of Au is deposited by sputter-coating (Jeol Auto fine-coater, Jeol Japan). A sputtering process of 45 s with setting at 20 mA was repeated 4 times to achieve a final thickness of the coating of about 40 nm, with 1 min waiting between each step to allow for sample cooling. Meanwhile, a glass coverslip (such as #1.5H) is prepared as a final substrate for the JeWell device by coating it with a thin layer of NOA73. A layer of NOA of about 20-30 µm thick is deposited on the coverslip by spin-coating and pre-cured under UV-light (30s in the same UV LED KUB2) so to become solid but still retaining adhesive properties. The Au-coated NOA structured film (still on the flat PDMS substrate) is flipped and placed in contact with the NOA-coated coverslip and gently pressed to ensure good contact. The NOA adhesive layer is then fully cured with a final step of UV flood exposure (1 min in the same UV LED KUB2 as previously) and the flat PDMS substrate can finally be peeled-off removing at the same time the portion of the metal film which is not coated on the NOA73 film.

Long term passivation of JeWell chips

This step is mandatory to avoid any adhesion of cells to the chips during the time of the experiments (>25 days) and to allow 3D culture of the cells. A solution of Lipidure® (CM5206, NOF America) at 0.5% (w/v) in pure ethanol is poured to completely cover the JeWell chips. Optionally, a 0_2 plasma cleaning of the coverslip (5min) has be done before. The JeWell chips covered with Lipidure solution is out-gassed (5-10 min in a vacuum jar evacuated to 5-10

mbar. Then, the ethanol-Lipidure solution is allowed to completely be evaporated under a sterile hood (>2 hours) in order to form a coating with same molecular structure as polar group of phospholipids. Before cells seeding, JeWell chips are rinsed with PBS, out-gassed as previously, and finally filled with cell culture medium.

Stem cell lines and their maintenance.

The human embryonic stem cell lines (hESCs) used for the experiments were H1 (WiCell Research institute, Inc. Madison, WI, USA) and K21 (lifeact-GFP, H2B-mCherry) (gift from Orly Reiner's lab, Weizmann Institute, Israel). Both cell lines used were on early passage number and confirmed to be contamination free.

We used hPSC-qualified Matrigel™ (354277, BD Biosciences) as the basement membrane matrix to culture and maintain the cells in the maintenance medium mTeSR™1 medium (05850, StemCell™ Technologies) for H1 and RSeT™ medium for K21 (05978, StemCell™ Technologies). The 80% confluent H1 cultures were passaged using Dispase (07923, StemCell™ Technologies) . We used TrypLE™ Express Enzyme (12605028, Thermofisher scientific) for K21 cultures. Gentle mechanical scrapping detached the cells. We resuspended them in fresh medium before to be re-plated on Matrigel™ coated wells.

Embryoid body formation in JeWells

For formation of embryoid bodies (EB) in JeWells, we dissociated the hESCs into single cell suspension by enzymatic with ReLeSR™ (05872, StemCell™ Technologies) for about 9 minutes. The hPSC cells were suspended at a concentration of 0.5 million cells/ml in EB formation medium supplied in STEMdiff™ Cerebral Organoid Kit (08570, StemCell™ Technologies) supplemented with 10 µM Y27632 (72304, Calbiochem, Merck Millipore) and seeded onto the JeWells. The cells were incubated for 10 minutes to allow adequate number of cells to enter per JeWell. Then we washed the chips with DMEM/F12 medium to remove excess cells. We incubated in EB formation medium supplemented with 10µM Y27632 for 24 hours. The neuroectoderm differentiation of EBs in JeWells was then initiated after 24 hours of cell seeding and/or when the EBs where ≥ 120µm in size.

Induction of neuroectoderm from hESCs in JeWells

To induce neuroectoderm differentiation, the embryoid bodies were cultured in STEMdiff™ Cerebral Organoid Kit (08570, StemCell™ Technologies) according to the manufacturer's instructions with slight modifications: when the EBs in JeWells reached ≥ 120µm in size we induced them to neuroectoderm using the induction medium from Cerebral Organoid Kit for 4 days. On day 5, the induction medium was removed and the induced EBs were embedded in 100% hPSC-qualified Matrigel™ (354277, BD Biosciences) for 30 mins. They were then allowed to undergo neural expansion using expansion medium from Cerebral Organoid Kit for 3 days.

Formation and growth of intestinal organoids in JeWells

The hESCs H1cell line was used to generate intestinal organoids. The induction of cells was done using STEMdiff™ Intestinal Organoid Kit (05140, StemCell™ Technologies) according to the manufacturer's instructions with slight modifications: H1 cells were seeded as cell aggregates of >200µm on Matrigel™ coated 24-well plate and allowed to reach ~90% confluence. At confluence, the cells were induced to definite endoderm for three days followed by mid/hindgut differentiation for next 6 days. Once the mid/hindgut differentiation was achieved the cells were dissociated as clumps of around 50-75µm by physical pipetting and seeded at a high density to cover all the JeWells. The aggregates were incubated for 15

minutes to allow adequate number of aggregates to enter the JeWells. Then the JeWells were washed with DMEM/F12 medium to remove excess cells and coated with Corning® Matrigel™ Growth Factor Reduced (GFR) Basement Membrane Matrix, Phenol Red-Free (356231, Corning) for 30 minutes. Once the Matrigel™ has solidified, the cell aggregates were supplied with intestinal organoid growth medium to generate intestinal organoids for 8-9 days. The medium was change every other day to keep the culture healthy.

For long-term culture of intestinal organoids in JeWells (20 days), pre-formed intestinal organoids in conventional culture system were passaged and broken into small clumps and seeded into JeWells in a similar way as described above. The JeWells were supplemented with fresh intestinal organoid growth every alternate day till required.

Primary rat hepatocytes isolation and seeding in JeWells

Hepatocytes were harvested from male Wistar rats by the two-step collagenase perfusion method as described by Seglen et al.[34]. Animals were handled according to the protocol established by Institutional Animal Care and Use Committee (IACUC) approved by the IACUC committee of National University of Singapore. Each isolation yielded >108 cells, with the viability ranging from 75-90% as tested by Trypan Blue exclusion assay. $0.15x10^6$ cells/ml suspended in cold hepatocytes William's E culture media (A1217601, Thermofisher scientific) supplemented with 1 mg/ml BSA (A7906,Sigma-Aldrich), 100nM Dexamethasone (D4902,Sigma-Aldrich), 2mM L-Glutamine (25030081, Thermofisher scientific), 0.3µg/ml of insulin (I9278, Sigma-Aldrich), 50µg/ml linoleic acid (L1376, Sigma-Aldrich), 100 units/ml penicillin and 100µg/ml streptomycin (15140122, Thermofisher scientific) were seeded as previously described per JeWell chip and the chips placed in the incubator for 5-10min to allow for the cells to settle. The dishes were then swirled, and the supernatant was collected to remove the floating cells. 1ml of fresh hepatocytes culture medium was added to the JeWell chip and were left to incubate during 2 to 4 days before fixation and immunostaining.

Cancer cell lines seeding in JeWells and formation of spheroids

HCT116 cells, colorectal cancer cells, were maintained in RPMI 1640 media (Invitrogen, 11875093) supplemented with 10% FBS (10082147, Invitrogen), 100 U/mL Penicillin-Streptomycin (15070063, Invitrogen) and 10mM / mL of Hepes (15630080, Invitrogen) at 37°C and 5% CO2. After trypsinization, the cells were suspended in complete 20% FBS DMEM (11965092, Invitrogen) media and the cell suspension was adjusted to $0.5X10^6$ cells/ml. 1ml of cell suspension was placed in 35mm JeWell plates for 10 mins to get approximately 80 cells per JeWell. The cell suspension was removed, washed once with DPBS (14190250, Invitrogen) and 2ml complete 20% FCS DMEM media was added to the plate. The media was changed on day 3 and day 6. The cells were fixed at day 10 for immunostaining.

Encapsulated cysts of stem cells culture and seeding in JeWells

Encapsulated cysts of hiPSC line IMAGINEi004 stem cells, were produced according to the protocol described in[35]. They were kindly provided by TreeFrog Therapeutics https://treefrog.fr/ in alginate capsules produced according to the system described in [36]. The cell/matrix suspension was entrapped inside a closed and permeable micro-sphere. They were cultured in mTeSR1 culture medium within T-flasks and maintain in a cell culture incubator at 37°C at 5% CO_2. The medium (mTeSR1) was supplemented with 10 µM Y-27632 for ROCK inhibition during the first 24h of cultures. Medium culture were change every day until day 6. The encapsulated cyst were provided fixed in PBS. The capsules were removed by incubating them in EDTA solution for 2 min (1 µM) and then stored in PBS + 0.1 tween20

before staining according to the protocol detailed below and seeding into JeWell chips. The stained cysts were seeded in square JeWells with 250 micron top opening at 1000 cyst/ml.

Organoids immunofluorescence staining for imaging (all organoids)

Organoids/spheroids in JeWell chips were fixed for 20 minutes in 4% paraformaldehyde (28906, Thermofisher scientific) at room temperature. IN the case of the capsules, we dissolved the alginate membrane using EDTA (10 mM) for 1 min at RT. The 3D cultures permeabilized for 24 hours in 1% Triton X-100 (T9284, Sigma Aldrich) solution in sterile PBS at 4°C on an orbital shaker, followed by 24 hours incubation in blocking buffer (2% bovine serum albumin BSA (37525, Thermofisher scientific) and 1% Triton X-100 in sterile PBS) at 4°C on an orbital shaker. Samples were then incubated with primary antibodies (Suppl Table1 for references and dilutions) diluted in antibody dilution buffer (2% BSA, 0.2% Triton-X 100 in sterile PBS) at 4°C for 48 hours. The samples were then rinsed 3 times with washing buffer on an orbital shaker (3% NaCl and 0.2% Triton-X 100 in sterile PBS) and incubated with secondary antibodies, donkey anti-mouse IgG-Alexa Fluor® 488 (A21202, Invitrogen, 1:500), donkey anti-goat IgG-Alexa Fluor® 633 (A21245, Invitrogen, 1:500), 0.5µg/ml DAPI (62248, Thermofisher scientific) and Alexa Fluor® 488 phalloidin (A12379, Thermofisher scientific, 1:200) at 4°C for 24 hours on an orbital shaker followed by 5 rinsing steps with washing buffer. The samples were finally washed following similar washing steps as after primary antibody incubation and mounted using RapiClear® 1.52 (RC 152001, Sunjin lab) pre-warmed at 37˚c.

Automated cell counting in JeWells after seeding

We imaged the JeWell Chip in transmitted bright field mode using the Metamorph ScanSlide module at 20X magnification just after the seeding and rinsing steps. The positions of the individual wells were automatically identified on the stitched image. We then cropped the stitched image into sub images containing a single well by threshold detection of the bright top aperture of each well. All the detection was performed using OpenCV-Python. We then trained a convolutional neural network for biomedical image segmentation published by the computer science department of the University of Freiburg U-Net using 200 raw images that we manually annotated. The training dataset was artificially augmented (3 times) applying transformations to the original images. We then estimated the area Ac per cells by using a linear regression between the segmented area predicted by the U-net per well and the ground truth number cell in the training set. We computed the number of cells per wells dividing the total predicted segmentation area by Ac. We found an error of around 6% as compared to the ground truth (Supplementary Figure 5). (N=200 wells). Once trained, the cell counting process by the U-net network is almost immediate.

Automated acquisition process

The microscope, the motorized stages, and the Multi-Dimensional Acquisition (MDA) process were controlled by MetaMorph software (Molecular Device). A dedicated home-made plugin (Visual basic) integrated into Metamorph allowed to control the soSPIM beam steering unit and therefore the sample illumination. It especially enabled to synchronize the 3D position of the light-sheet (after reflection onto the 45° mirror) with the objective's axial movement and the acquisition process to ensure a proper superposition of the excited and imaged plane for optimal 3D imaging as described in Galland et al.[19]. The light-sheet calibration and repositioning during multi-position acquisition are performed using brightfield images of the JeWells. The calibration is performed semi-automatically, by simply user-drawing a line in the direction of the mirror, at the in-focus position, which is clearly visible from a bright-field image of a JeWell. Repeating this process for two different Z positions (eg. at the top and at

the bottom of the JeWell), allows calibrating the position of the light-sheet on the mirror with respect to the Z position, and guarantees a perfect alignment of the light sheet with the focal plane of the objective. The precise arrayed structure of the JeWells ensures the mirrors orientations to remain the same for all the JeWells contained in a JeWell chip, facilitating multi-position acquisition as long as JeWells are repositioned exactly at the same position in the camera field of view. Indeed, the soSPIM architecture couple the lateral (XY) JeWell position with the axial (Z) position of the light-sheet (**Supplementary Figure 4a**). To control the exact positioning of the JeWell in the camera field of view for both automatic multi-position acquisition and drift correction during time-lapse acquisition we developed a fully automatic positioning tool. It relied on the cross-correlation of the JeWells high-contrasted brightfield images in between a reference position on which the soSPIM imaging synchronization has been performed and the JeWell that will be imaged with a subpixel resolution (**Supplementary Figure 4b**). The positioning accuracy was estimated to be less than 45.8 nm for a computational time of 188 ± 13 ms (with an image binning factor of 4) ensuring optimal 3D soSPIM imaging of all positions (and time-point) defined with neglectable impact on the acquisition duration. To ease and fasten multi-dimensional acquisition set-up leveraging the arrayed structures of JeWells, we developed a 4 steps process as described in **Supplementary figure 4c**. It relies on (*step 1*) the acquisition of a brightfield preview of the whole JeWell chip, (step 2) the automatic JeWells positions detection and (*step 3*) the interactive selection of the positions to be imaged, before (*step 4*) the screen of those position according to the acquisition's parameters preliminary defined (frequency, excitation wavelengths, Z series, …). The integration of the repositioning tool within this acquisition pipeline ensures optimal 3D soSPIM imaging of all the positions and time-points of the screen. Overall, it took 25 min to set-up a screen on 321 positions (*steps 1* to *3*) including 20 min for the chip acquisition preview.

Nuclei segmentation by StarDist

The 3D segmentation of nuclei was performed using StarDist[37] convolutional neural network (CNN). All the image stacks were resized from 2048*2048 to 614*614, keeping the number of planes constant, to allow StarDist training on a standard desktop computer equipped with a Geforce RTX 2080 Ti NVIDIA GPU with 11Go of graphical memory. We manually annotated 7 organoids using Napari[38], corresponding to 471 frames and 5,274 3D nuclei. After resizing, the median size of our annotated nuclei was 28*27*7 voxels. We used a patch size of 96*96*24 voxels to guarantee that the network's field of view encapsulates at least one nucleus. Data augmentation was performed with random flips, rotations, and intensity modifications, and we used 85% of the data set for training and 15% for validation of the network predictions. Training used 400 epochs and required approximately 4 hours. Prediction of a complete 3D stack required 40 seconds (4 seconds for resizing and 36 ± 21 seconds for the StarDist prediction **Supplementary Movie 2**). Segmentation applied to 96 organoids resulted in 55,976 nuclei and has been used to measure intensities of transcription factors for all organoids. Distributions of the nuclei volume were computed using the MorphoLibJ[39] plugin.

Detection of Ki67 classes, mitosis, and apoptosis in 3D by YOLOv5

The detection of Ki67 classes[20] (Early G1, G1/S/G2, Mitosis) and apoptosis and mitosis (DAPI) events was performed using the YOLOv5 CNN published by ZeroCostDL4Mic, run on our GPU resources (NVIDIA Quadro RTX6000 24GB) (**Supplementary Figure 6a**). For the Ki67 classes, a custom-made image analysis algorithm based on local thresholding and morphology

mathematics has been implemented under ImageJ to help for the detection of the Ki67 positive region (surrounding boxes, **Supplementary Movie 3**) following by a manual step of classification. This has been done on 13 images stacks of 71 z-planes of the Ki67 signal only. For the mitosis/apoptosis detection on DAPI signal, 28 image stacks of 71 z-planes were manually annotated by selecting 30x30 pixels bounding boxes around the central plane of the apoptosis and 50x50 pixels bounding boxes around the central plane of the mitosis using ImageJ. For both type of detection, these annotated stacks constituted the ground truth of the training dataset, representing a total of 35000 positive region in 2D for Ki67 signal, and for DAPI signal a total of 344 mitosis and 1,123 apoptosis 2D region. For mitosis/apoptosis only, an additional data augmentation was performed using image flipping and rotation, representing 4,128 2D region of mitosis and 13,476 apoptosis. We used 90% of the data set for training and 10% for validation of the network prediction. After training, the prediction of a single plan image took 20msec and around 1sec for a full 3D stack. The AI network identified bounding boxes around individual events in each plan independently (2D). 3D detection was achieved using a custom MATLAB routine identifying and fusing the same event detected in consecutive planes. The centre coordinates of each 3D box were plotted as a localization map. We measured the confusion matrix by comparing the overlap between the predicted bounding box with the ground truth (**Supplementary Figure 6a**).

Classification of organoid shapes by DenseNet121

Raw images of global organization of organoids based exclusively on the actin (Phalloidin) and nuclei (DAPI) staining were analyzed using deep learning algorithms developed for image classification. We manually distinguished 2 classes of organoids: 'O-shape' organoids displaying a spherical global shape, and 'B-shape' ones for which an external streak surrounding by 2 cellular lobes tending to join can be clearly distinguished. We analyzed 132 (2048*2048*64 planes) 3D images using DenseNet121[26] CNN for classify the 3D images into those two classes (see **Supplemental Figure 6b**). To accommodate the memory constraint of the graphics card (Geforce RTX 2080 Ti NVIDIA GPU with 11Go of graphical memory), we resized the whole dataset to 128*128*64, a size where the structures are still roughly distinguishable. A 5-fold cross-validation was performed with a 60/20/20 split for training, validation and test set definition. Each fold was launched with a DenseNet121 implementation with Adam optimizer[40]. To counterbalance large imbalance between the two classes, each training iteration was launched with a batch consisting of as many 'O-shape' as 'B-shape'. After training, the prediction of the classes among a set of 130 organoids took less than 1s in total, with 99% of accuracy. Subsequently, each 'O-shape' organoids were analyzed for internal streaks segmentation.

Segmentation of internal streaks by 3D U-Net

Classified 'O-shape' organoids were proceeded for the segmentation of internal streak based only on morphological staining (DAPI and Phalloidin) to permit the detection of morphological patterns independently of gene expression level (**Supplementary Figure 6c**). The 3D dataset was first resized to 1024 * 1024 * 71, and each image plane was manually segmented using 3D Slicer software[41], giving a ground truth mask. Original image and corresponding masks were again resized to 256*256*71 for faster testing of deep learning algorithms. The same 5-fold cross-validation procedure described previously were applied using 3D U-Net[42] CNN. The prediction produced probability maps of size 256 * 256 * 71 for each image. An arbitrary threshold of 0.5 was applied to each map, resulting in a binary streak segmentation mask. Once the network trained, the streak detection with the generation of the corresponding

mask took approximatively 5 seconds for each organoid. A 3D connected components algorithm was used to label each voxel of the binary masks. Most of segmented objects seemed relevant for internal streaks as showed in **Figure 6** and **Supplementary Figure 6**.

Image analysis of intestinal organoids for CDX2 and E-cadherin signals

The 20x resolution (air objective, N.A 0.75) image stacks of 100 intestinal organoids were automatically analysis using a custom-made ImageJ routine based on the maximum intensity projection followed by thresholding and morphological mathematic operations to first classify organoids positive for CDX2 transcription factor ($CDX2^+$) and then, after the second round of acquisition, to delineate the region of positive E-cadherin ($E\text{-}cad^+$) clusters. These 2 steps of analysis have been launched just after each round of acquisitions and took less than 10 minutes each. The positive organoids and region of interest have been registered to allow the following acquisition using a higher resolution objective (60X, WI, N.A 1.27).

JeWells peeling and real-time PCR

Organoids were released from the JeWells by peeling off the top layer. Organoids were then flushed twice with DMEM/F-12 1:1 (Gibco) and collected within a microcentrifuge tube. Total RNA was extracted from these organoids using RNeasy Plus Micro Kit (74034, QIAGEN) according to the manufacturer's protocol. 450ng of total RNA was used to form the cDNA using cDNA synthesis kit (SensiFAST™, BIO-65054, Bioline). qPCR was performed using FastStart Universal SYBR Green Master (ROX) mix on a CFX96 Touch Real-Time PCR detection system (Bio-Rad). Primers sequences for the 12 genes tested are listed on the **Table 1**. GAPDH was used as a housekeeping gene.

REFERENCES

1. Kim, J., Koo, B. K. & Knoblich, J. A. Human organoids: model systems for human biology and medicine. *Nature Reviews Molecular Cell Biology* (2020) doi:10.1038/s41580-020-0259-3.
2. Takebe, T. & Wells, J. M. Organoids by design. *Science (80-.).* **364**, 956–959 (2019).
3. Kratochvil, M. J. *et al.* Engineered materials for organoid systems. *Nat. Rev. Mater.* **4**, 606–622 (2019).
4. Rossi, G., Manfrin, A. & Lutolf, M. P. Progress and potential in organoid research. *Nat. Rev. Genet.* **19**, 671–687 (2018).
5. O'Connell, L. & Winter, D. C. Organoids: Past learning and future directions. *Stem Cells Dev.* **29**, 281–289 (2020).
6. Vives, J. & Batlle-Morera, L. The challenge of developing human 3D organoids into medicines. *Stem Cell Research and Therapy* (2020) doi:10.1186/s13287-020-1586-1.
7. Busslinger, G. A. *et al.* The potential and challenges of patient-derived organoids in guiding the multimodality treatment of upper gastrointestinal malignancies. *Open Biol.* (2020) doi:10.1098/rsob.190274.
8. Lukonin, I. *et al.* Phenotypic landscape of intestinal organoid regeneration. *Nature* (2020) doi:10.1038/s41586-020-2776-9.
9. Renner, H. *et al.* A fully automated high-throughput workflow for 3d-based chemical screening in human midbrain organoids. *Elife* (2020) doi:10.7554/eLife.52904.

10. https://bioengineeringcommunity.nature.com/posts/intestinal-regeneration-lessons-from-organoids.

11. Rios, A. C. & Clevers, H. Imaging organoids: A bright future ahead. *Nature Methods* (2018) doi:10.1038/nmeth.4537.

12. Dekkers, J. F. *et al.* High-resolution 3D imaging of fixed and cleared organoids. *Nat. Protoc.* **14**, 1756–1771 (2019).

13. Wan, Y., McDole, K. & Keller, P. J. Light-sheet microscopy and its potential for understanding developmental processes. *Annual Review of Cell and Developmental Biology* (2019) doi:10.1146/annurev-cellbio-100818-125311.

14. Serra, D. *et al.* Self-organization and symmetry breaking in intestinal organoid development. *Nature* (2019) doi:10.1038/s41586-019-1146-y.

15. Eismann, B. *et al.* Automated 3D light-sheet screening with high spatiotemporal resolution reveals mitotic phenotypes. *J. Cell Sci.* **133**, 1–20 (2020).

16. Voleti, V. *et al.* Real-time volumetric microscopy of in vivo dynamics and large-scale samples with SCAPE 2.0. *Nat. Methods* (2019) doi:10.1038/s41592-019-0579-4.

17. Yang, B. *et al.* Epi-illumination SPIM for volumetric imaging with high spatial-temporal resolution. *Nat. Methods* (2019) doi:10.1038/s41592-019-0401-3.

18. Maioli, V. *et al.* Time-lapse 3-D measurements of a glucose biosensor in multicellular spheroids by light sheet fluorescence microscopy in commercial 96-well plates. *Sci. Rep.* (2016) doi:10.1038/srep37777.

19. Galland, R. *et al.* 3D high- and super-resolution imaging using single-objective SPIM. *Nat. Methods* **12**, 641–644 (2015).

20. Sun, X. & Kaufman, P. D. Ki-67: more than a proliferation marker. *Chromosoma* (2018) doi:10.1007/s00412-018-0659-8.

21. Lancaster, M. A. *et al.* Cerebral organoids model human brain development and microcephaly. *Nature* (2013) doi:10.1038/nature12517.

22. Hříbková, H., Grabiec, M., Klemová, D., Slaninová, I. & Sun, Y. M. Calcium signaling mediates five types of cell morphological changes to form neural rosettes. *J. Cell Sci.* **131**, (2018).

23. Fedorova, V. *et al.* Differentiation of neural rosettes from human pluripotent stem cells in vitro is sequentially regulated on a molecular level and accomplished by the mechanism reminiscent of secondary neurulation. *Stem Cell Res.* (2019) doi:10.1016/j.scr.2019.101563.

24. Meinhardt, A. *et al.* 3D reconstitution of the patterned neural tube from embryonic stem cells. *Stem Cell Reports* (2014) doi:10.1016/j.stemcr.2014.09.020.

25. Chandrasekaran, A. *et al.* Comparison of 2D and 3D neural induction methods for the generation of neural progenitor cells from human induced pluripotent stem cells. *Stem Cell Res.* (2017) doi:10.1016/j.scr.2017.10.010.

26. Huang, G., Liu, Z., Van Der Maaten, L. & Weinberger, K. Q. Densely connected convolutional networks. in *Proceedings - 30th IEEE Conference on Computer Vision and Pattern Recognition, CVPR 2017* (2017). doi:10.1109/CVPR.2017.243.

27. Karzbrun, E., Kshirsagar, A., Cohen, S. R., Hanna, J. H. & Reiner, O. Human brain organoids on a chip reveal the physics of folding. *Nat. Phys.* (2018) doi:10.1038/s41567-018-0046-7.

28. Driehuis, E. *et al.* Pancreatic cancer organoids recapitulate disease and allow personalized drug screening. *Proc. Natl. Acad. Sci. U. S. A.* (2019) doi:10.1073/pnas.1911273116.

29. Yoshida, S., Miwa, H., Kawachi, T., Kume, S. & Takahashi, K. Generation of intestinal organoids derived from human pluripotent stem cells for drug testing. *Sci. Rep.* (2020) doi:10.1038/s41598-020-63151-z.

30. Beccari, L. *et al.* Multi-axial self-organization properties of mouse embryonic stem cells into gastruloids. *Nature* (2018) doi:10.1038/s41586-018-0578-0.

31. Sorrentino, G. *et al.* Mechano-modulatory synthetic niches for liver organoid derivation. *Nat. Commun.* (2020) doi:10.1038/s41467-020-17161-0.

32. Kumar, S. V. *et al.* Kidney micro-organoids in suspension culture as a scalable source of human pluripotent stem cell-derived kidney cells. *Dev.* (2019) doi:10.1242/dev.172361.

33. Perche, F. & Torchilin, V. P. Cancer cell spheroids as a model to evaluate chemotherapy protocols. *Cancer Biol. Ther.* (2012) doi:10.4161/cbt.21353.

34. Seglen, P. O. Preparation of Isolated Rat Liver Cells. *Methods Cell Biol.* (1976) doi:10.1016/S0091-679X(08)61797-5.

35. Quelennec, E. *et al.* Generation of two induced pluripotent stem cell lines IMAGINi004-A and IMAGINi005-A from healthy donors. *Stem Cell Res.* **48**, 101959 (2020).

36. Alessandri, K. *et al.* A 3D printed microfluidic device for production of functionalized hydrogel microcapsules for culture and differentiation of human Neuronal Stem Cells (hNSC). *Lab Chip* **16**, 1593–1604 (2016).

37. Weigert, M., Schmidt, U., Haase, R., Sugawara, K. & Myers, G. Star-convex Polyhedra for 3D Object Detection and Segmentation in Microscopy. *Proc. - 2020 IEEE Winter Conf. Appl. Comput. Vision, WACV 2020* 3655–3662 (2019) doi:10.1109/WACV45572.2020.9093435.

38. Sofroniew, N. *et al.* napari/napari: 0.4.9rc1. (2021) doi:10.5281/ZENODO.4905201.

39. Legland, D., Arganda-Carreras, I. & Andrey, P. MorphoLibJ: Integrated library and plugins for mathematical morphology with ImageJ. *Bioinformatics* (2016) doi:10.1093/bioinformatics/btw413.

40. Kingma, D. P. & Ba, J. L. Adam: A method for stochastic optimization. in *3rd International Conference on Learning Representations, ICLR 2015 - Conference Track*

Proceedings (2015).

41. Fedorov, A. *et al.* 3D Slicer as an image computing platform for the Quantitative Imaging Network. *Magn. Reson. Imaging* (2012) doi:10.1016/j.mri.2012.05.001.

42. Ronneberger, O., Fischer, P. & Brox, T. U-Net: Convolutional Networks for Biomedical Image Segmentation [2015; First paper exploring U-Net architecture.]. in *International Conference on Medical image computing and computer-assisted intervention* (2015).

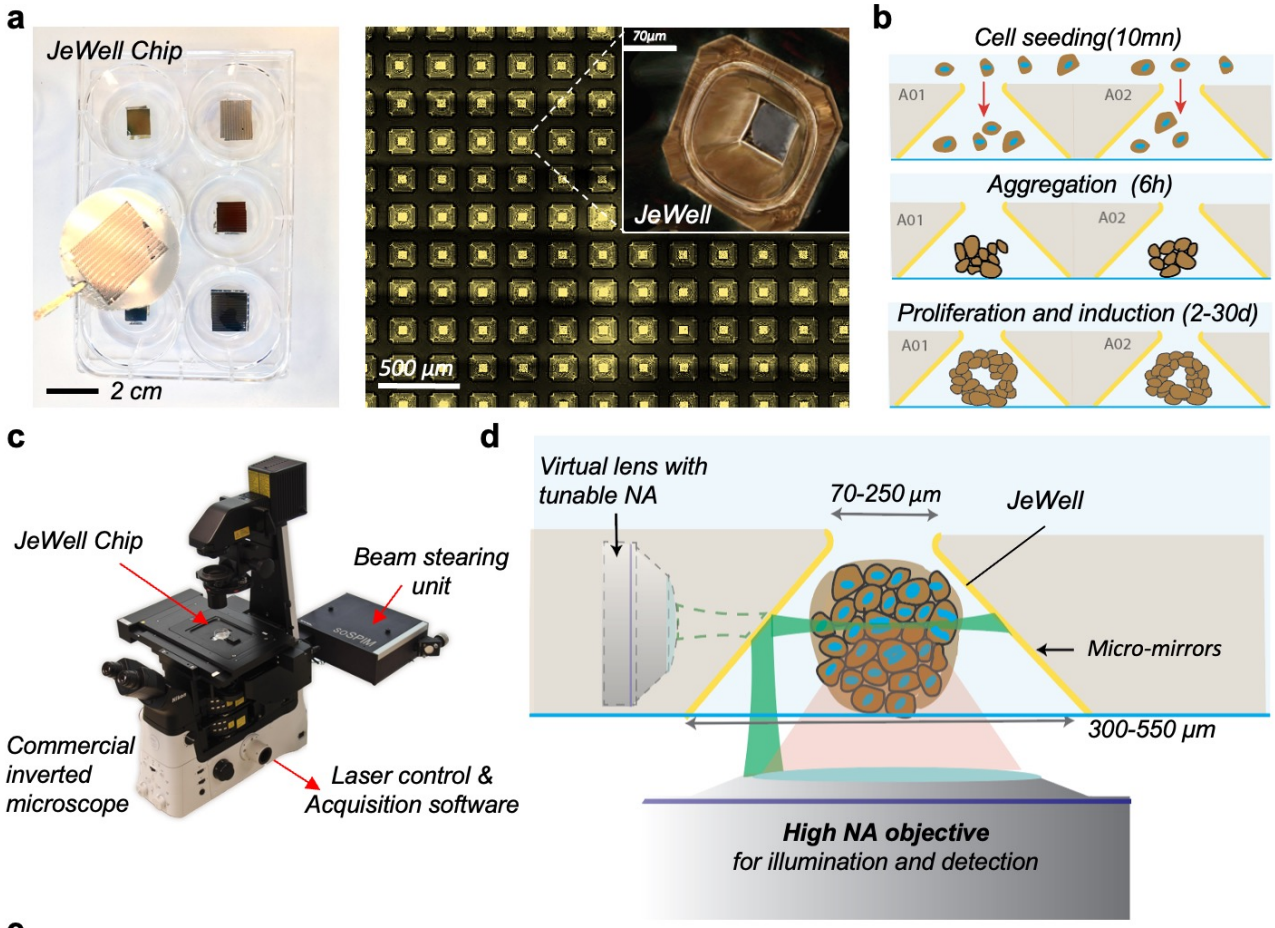

96 organoids, 70 z plans each, 3 wavelengths, 173GB of (2048x2048x70) stacks, 1h acquisition time

Figure 1:
Working principles. a. JeWell chips in a 6 well dish (left) and close-up image of the JeWells array with a density of 16 JeWells/mm^2 (right). Inset shows a zoom on a JeWell inverted pyramidal microcavities flanked with four 45° mirroring surfaces. **b.** Schematic of the seeding procedure. Dissociated cells are homogeneously seeded above the chip. They sediment inside the pyramids for 10 mins, then aggregate for the next hours and finally proliferate and differentiate for up to 30 days in the JeWell cavities. **c.** Photography the imaging set-up comprising a commercial inverted microscope, combined with JeWell chips, a laser scanning unit and its custom-made control software. **d.** Principles of the single objective selective plane illumination microscopy (soSPIM). The light-sheet perpendicular to the optical axis is created by reflection of the laser beam (green) onto the 45° mirrored surfaces of a JeWell, acting as a virtual second objective. The fluorescence emission (red) is then collected through the same objective. **e**. Representative gallery of 96 neuroectoderm organoids (median plane of the 3D stacks) labelled with Actin (gold), Sox2 (magenta) and DAPI (blue) acquired in an automated workflow in less than 1 hour.

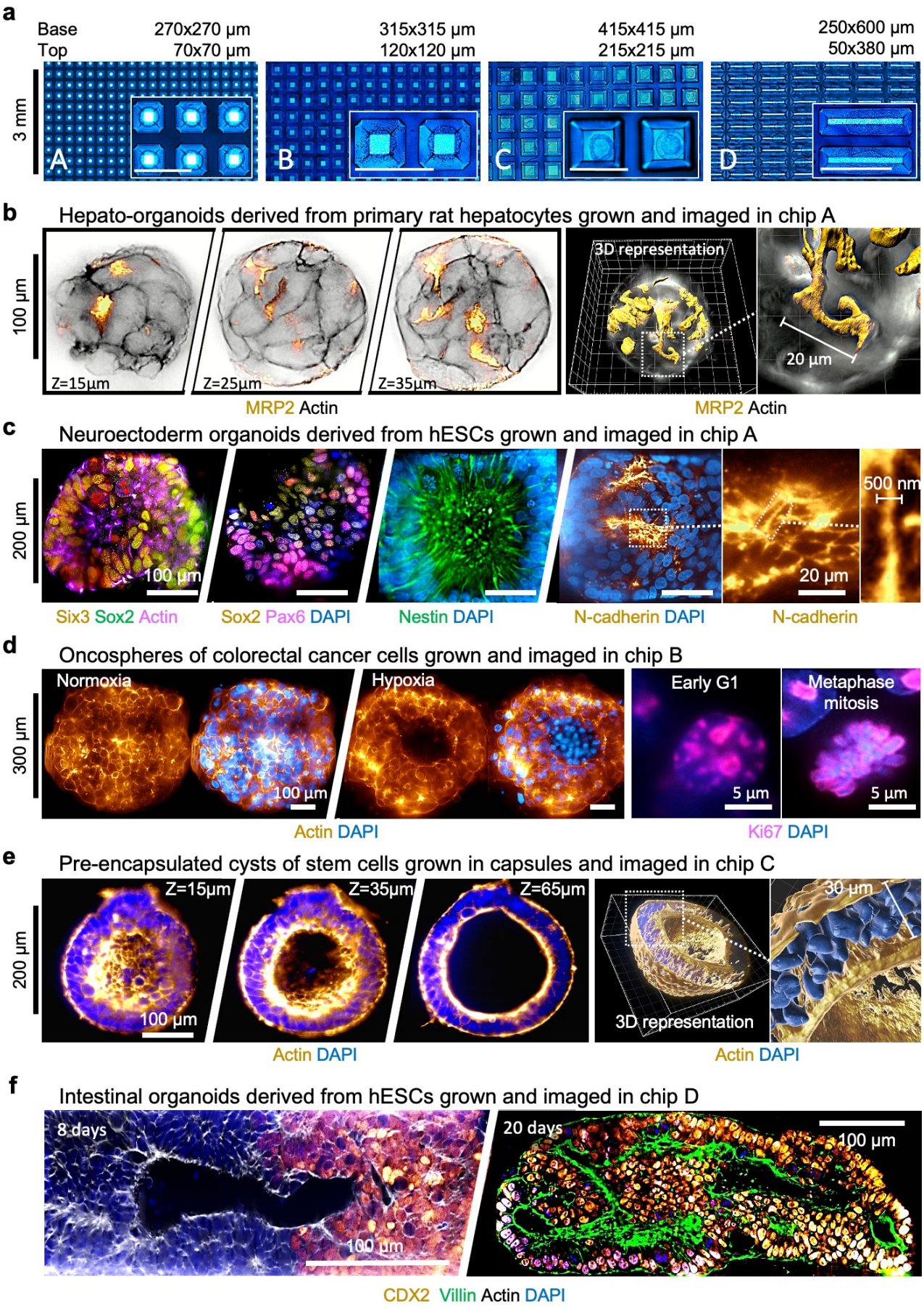
a
Base
Top
270x270 µm
70x70 µm
315x315 µm
120x120 µm
415x415 µm
215x215 µm
250x600 µm
50x380 µm
3 mm
A
B
C
D
b
Hepato-organoids derived from primary rat hepatocytes grown and imaged in chip A
100 µm
Z=15µm
Z=25µm
Z=35µm
3D representation
20 µm
MRP2 Actin
MRP2 Actin
c
Neuroectoderm organoids derived from hESCs grown and imaged in chip A
200 µm
100 µm
20 µm
500 nm
Six3 Sox2 Actin
Sox2 Pax6 DAPI
Nestin DAPI
N-cadherin DAPI
N-cadherin
d
Oncospheres of colorectal cancer cells grown and imaged in chip B
300 µm
Normoxia
Hypoxia
100 µm
Early G1
Metaphase mitosis
5 µm
5 µm
Actin DAPI
Ki67 DAPI
e
Pre-encapsulated cysts of stem cells grown in capsules and imaged in chip C
200 µm
Z=15µm
Z=35µm
Z=65µm
100 µm
3D representation
30 µm
Actin DAPI
Actin DAPI
f
Intestinal organoids derived from hESCs grown and imaged in chip D
8 days
100 µm
20 days
100 µm
CDX2 Villin Actin DAPI

Figure 2:

Matching JeWell chips to different sorts of organoids. a. Examples of JeWell cavities dimensioned to fit the size of the organoids (scale bars 500µm). It maximized the image quality, protected the organoids for external flux, allowed embedding in Extra-cellular matrix (Matrigel) and provided scaffolds for the organoid growth. **b** Representative examples of 3D stacks (60X, WI) and 3D reconstruction of primary rat hepatocyte aggregates stained for actin (grey) and MRP2 (canaliculi marker) (gold) after 4 days of culture (N=96). **c** Representative median plane images (60X, WI) of hESCs derived Neuroectoderm organoids (8 days old) immunolabeled for various transcription factors (as indicated). 3D rosettes could easily be identified with the N-cadherin rich core. Intra-rosette N-cadherin structures (<300nm) were visible (N=400). **d** Typical images (20X) of oncospheres (HCt116) (~ 200µm in diameter) grown in hypoxic conditions displayed a hypoxic center as compared to the normoxic conditions. The imaging resolution was fully capable of distinguishing proliferation stages (G0, G1, S, mitosis) based on Ki67 staining (N=400). **e.** Representative 3D stack (20X) and 3D reconstructions of hESCs cells pre-encapsulated in alginate capsules. The encapsulated cells were grown outside the JeWells and the capsules were seeded in pyramids with large top openings (215 µm). **f** Representative median plane (20x) of intestinal organoids derived from hESCs at day 8 (left) and day 20 (right). The intestines grew in rectangle grooves. They elongated along the long axis. Staining at early stage (D08) showed clustered expression of CDX2 that became ubiquitous at later stage organoids (D20) presenting Villin lining the central lumen (N=96). All images in the figure are raw images from soSPIM set up without any post-processing .

a Nuclei 3D segmentation

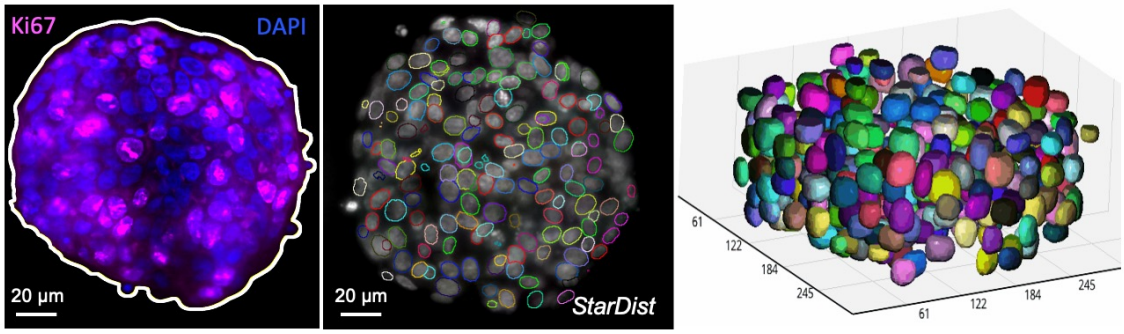

Organoid volume

DAPI-based nuclei 3D segmentation

b Proliferation stage quantification

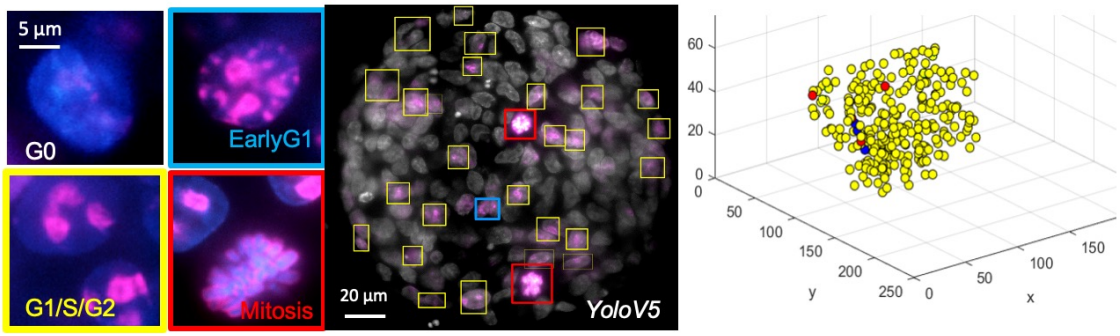

Ki67-based cell cycle classification

3D mapping within the organoid

c Quantification of a library of hundreds oncospheres

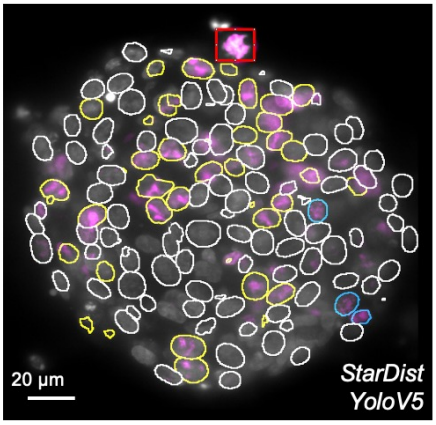

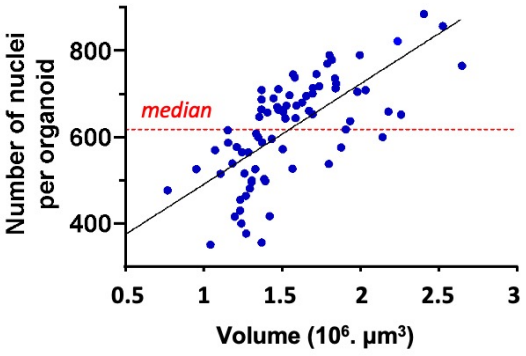

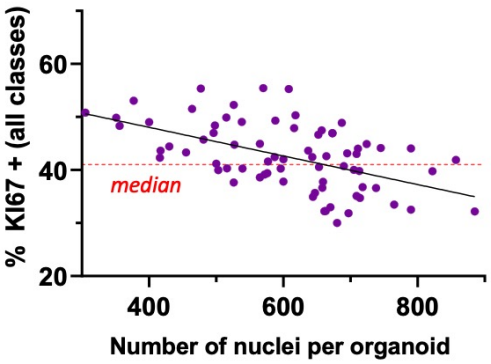

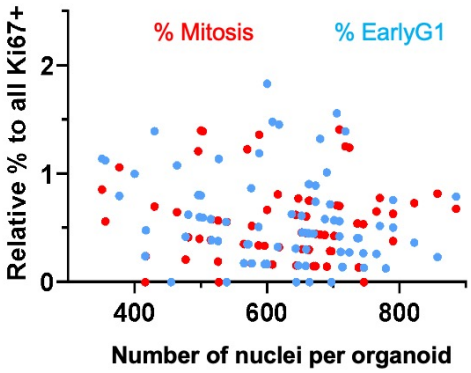

Figure 3:
Sub-cellular quantification of cell proliferation in oncospheres.
a. Image of the median plane of an oncosphere (HCT116) stained for nuclei (DAPI) and ki67 in normoxy conditions. The volume of the oncosphere is measured by thresholding the aggregate contour in 3D. Individual nucleus positions are obtained by segmenting the DAPI channel using the 3D StarDist neural network. 3D reconstruction of segmented nuclei by surface rendering. **b.** AI detection of three different stages of cell division based on the ki67 signal using YoloV5. The 3D localization of individual proliferating nucleus is represented in 3D by a sphere. The colors code for the proliferation stages (blue for Early G1, yellow for G1/S/G2, red for mitosis). **c.** Correlation between the predictions of both AI networks. The color code of the nuclei contours corresponds to the class of proliferation stages. The total number of nuclei linearly scaled with the approximated volume of the oncosphere. The fraction of cells in each proliferative state decreased proportionally to the total number of cells. However, there are no sign of arrest at any proliferation checkpoint as demonstrated by the constant proportion of each phase relative to the total number of proliferative cells. Each point represents one organoid.

a Division and mortality detection

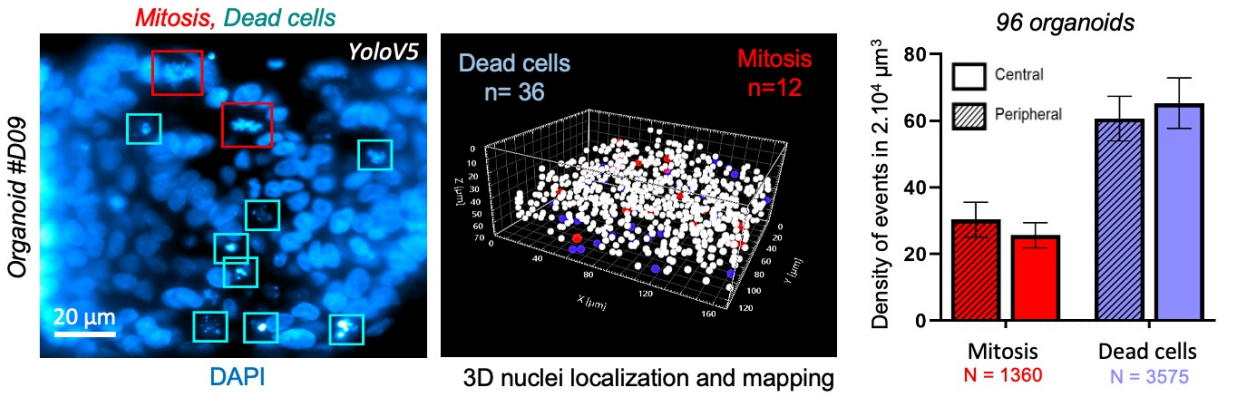

b Cellular phenotyping

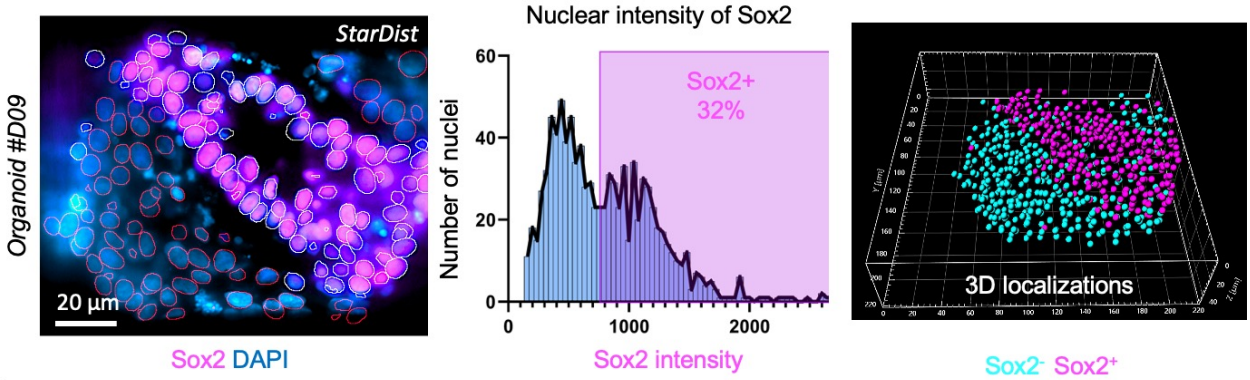

c 3D segmentation of multicellular patterns

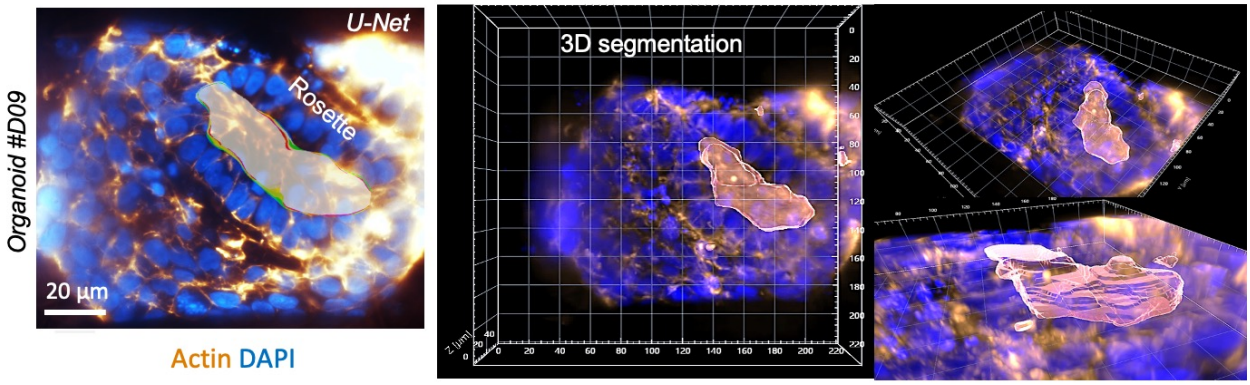

e Classification of the organoid morphologies

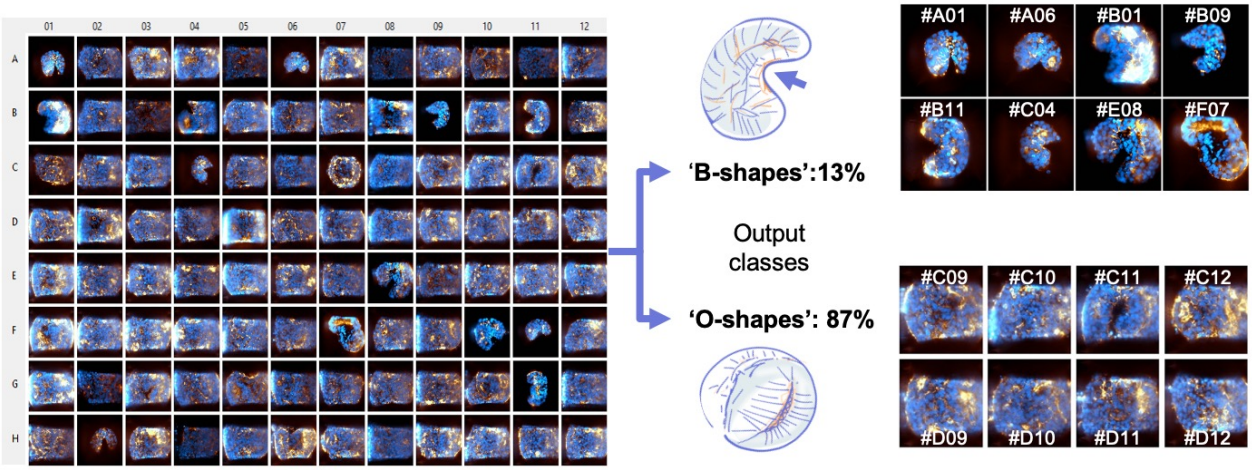

Figure 4: Multiscale analysis of neuroectoderm organoids.
a. Example of detection of mitosis and cell death based on DAPI signal using YoloV5 convolutional neuronal network (CNN). 3D localization of mitosis and cell death events within one full organoid. White: all nuclei (N=680) (detected by StarDist), blue: cell death (N=36) and red: mitosis (N=12). Comparison of the density of mitosis and cell death in the core vs the periphery of organoids (N=96) for the entire organoid collection. The density of events (out of 1,360 mitosis and 3,575 cell death) showed no significant differences between sub-volumes (2.10^4 μm^3) in the central and the peripheral regions. It suggests that the proliferation and cell death were homogeneously distributed within the organoids. **b.** 3D segmentation of the nuclei in neuroectoderm organoid using 3D StarDist CNN on DAPI signal. Bimodal distribution of the average intensity levels of Sox2 signals within each nuclei. Green contours correspond to $Sox2^-$ cells , red contours to $Sox2^+$ cells. 3D representation of the $Sox2^-$ (cyan) and $Sox2^+$ (purple) nuclei based on the cut-off derived from the histogram. $Sox2^+$ cells localized around the rosette. **c.** 3D segmentation of the streak regions of the rosettes based on actin structure (gold) were segmented using 3D U-net CNN. **d.** DenseNet121 CNN classification of the neuroectoderm organoid morphologies in 2 classes: B-shape or O-shape (N= 96). The classification of each organoid was achieved with 100% accuracy.

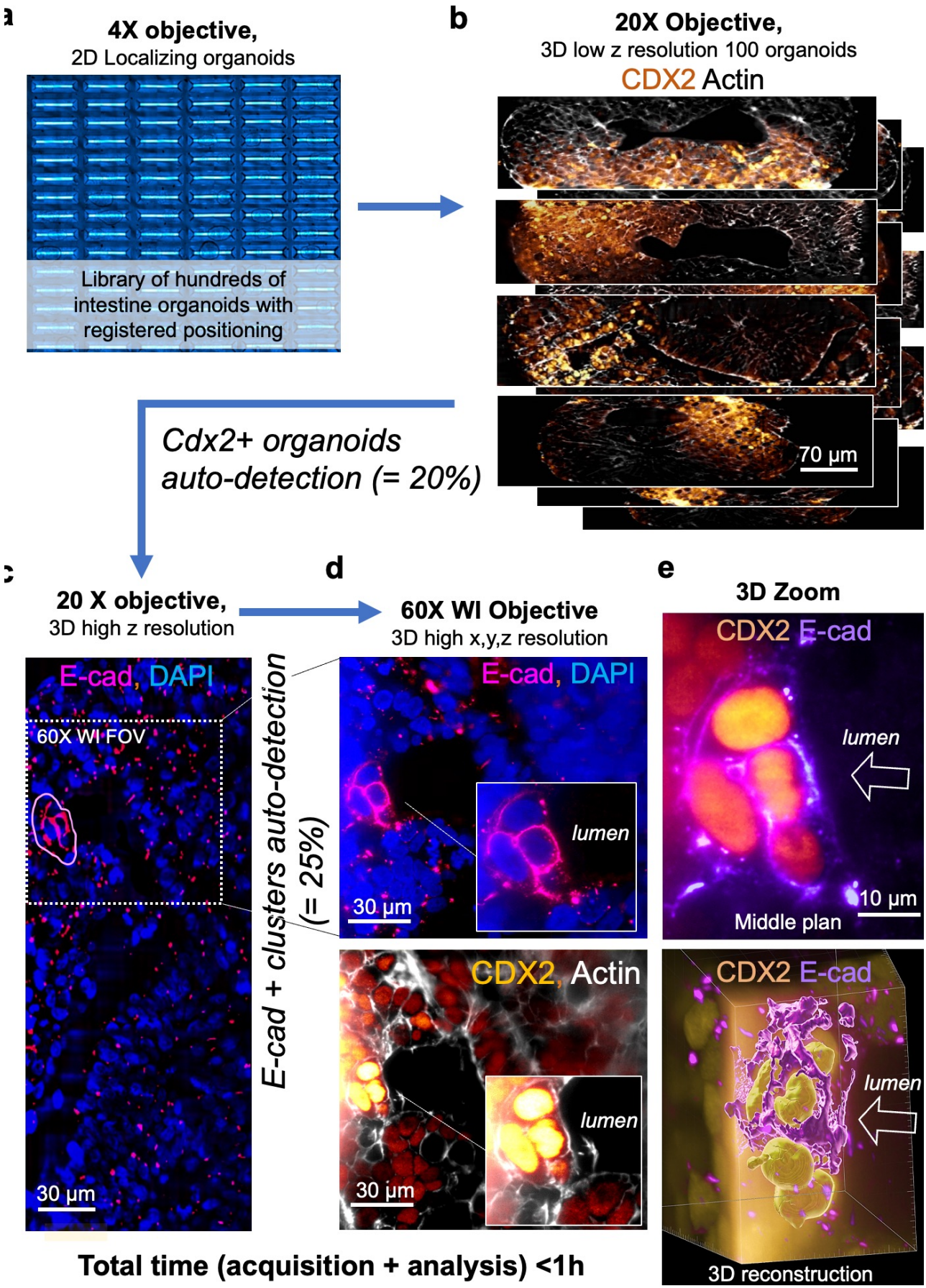
a
4X objective,
2D Localizing organoids
Library of hundreds of intestine organoids with registered positioning
b
20X Objective,
3D low z resolution 100 organoids
CDX2 Actin
70 µm
Cdx2+ organoids auto-detection (= 20%)
c
20 X objective,
3D high z resolution
E-cad, DAPI
60X WI FOV
30 µm
E-cad + clusters auto-detection (= 25%)
d
60X WI Objective
3D high x,y,z resolution
E-cad, DAPI
lumen
30 µm
CDX2, Actin
lumen
30 µm
e
3D Zoom
CDX2 E-cad
lumen
10 µm
Middle plan
CDX2 E-cad
lumen
3D reconstruction
Total time (acquisition + analysis) <1h

Figure 5: Efficient *rare events detection by multi-magnification imaging pipeline.*

a. A representative brightfield image using a 4x objective of a rectangular JeWell chip with intestinal organoids (Day 8). **b**. A collection of 100 intestine organoids with registered positions were imaged in less than 10 min using a 20X objective (air) in soSPIM (7 plans per organoid, step size of 10 microns, 2 channels : CDX2 and Actin). We automatically selected the CDX2 positive organoids (~ 20% of the whole batch, N=100). **c .** Rare clusters of E-cad+ cells (pink contour) were automatically detected by a second round of imaging of the selected CDX2+ organoids (20X with a higher Z resolution of 1 micron, 50 plans, 10 min) (= 25% of the CDX2+ organoids, =m5% of the whole batch). **d.** Optical zoom using a 60X, WI, 1.27 N.A objective on the selected field of views containing E-Cad+ clusters. The total time of the process was less than 1hour. **e.** The final high-resolution imaging enabled to reconstruct and to localize in 3D the E-cad^{+} junctions of the CDX2^{+} cells.

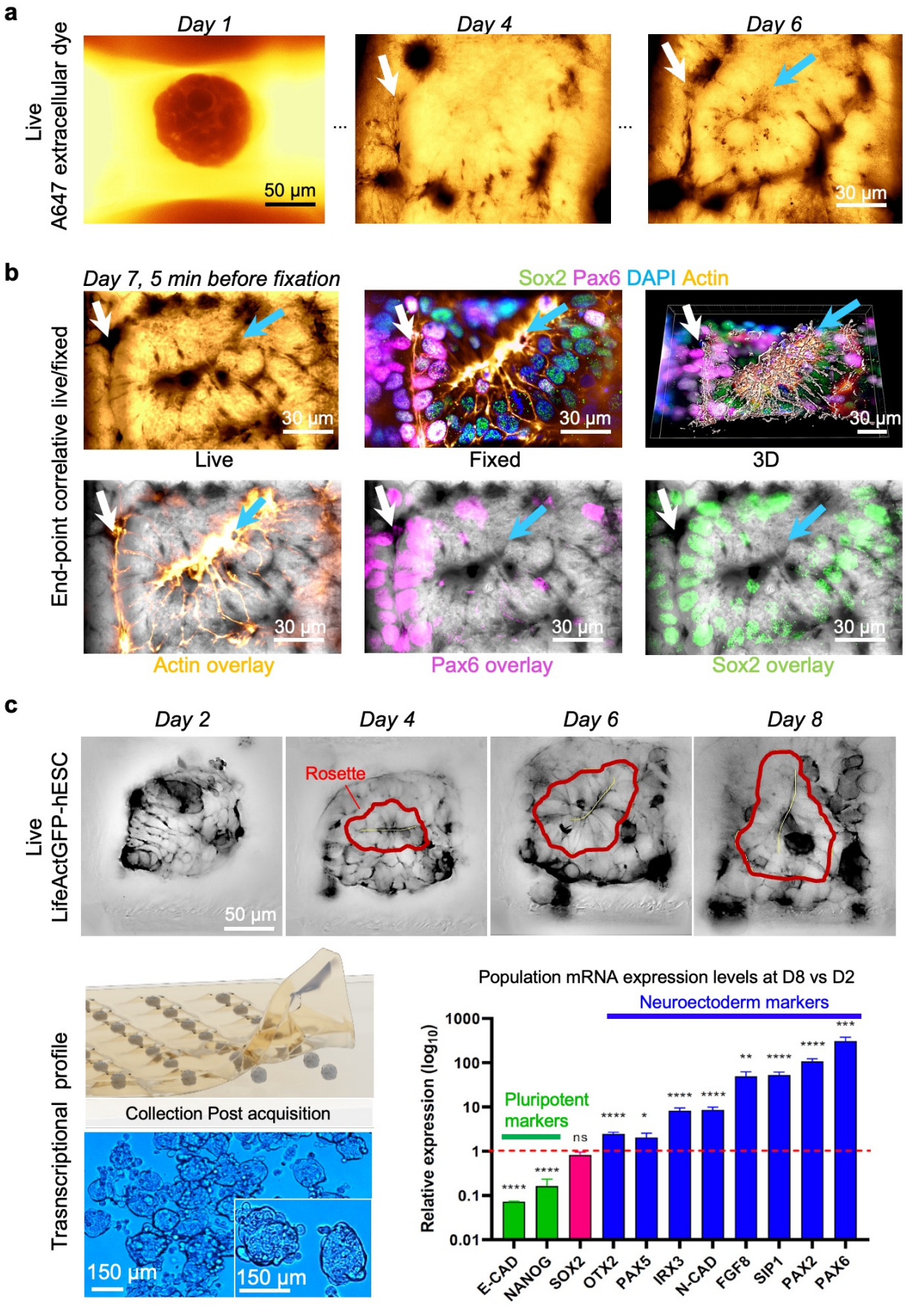
a
Live
A647 extracellular dye
Day 1
Day 4
Day 6
50 µm
30 µm
b
End-point correlative live/fixed
Day 7, 5 min before fixation
Sox2 Pax6 DAPI Actin
30 µm
Live
Fixed
3D
Actin overlay
Pax6 overlay
Sox2 overlay
c
Live
LifeActGFP-hESC
Day 2
Day 4
Day 6
Day 8
Rosette
50 µm
Trasnscriptional profile
Collection Post acquisition
150 µm
Population mRNA expression levels at D8 vs D2
Neuroectoderm markers
Pluripotent markers
Relative expression (log10)
1000
100
10
1
0.1
0.01
ns
E-CAD
NANOG
SOX2
OTX2
PAX5
IRX3
N-CAD
FGF8
SIP1
PAX2
PAX6

Figure 6. Correlative imaging of live vs transcription factors expression.

a. Live imaging performed on neuroectoderm organoid during 7 days of development. Alexa647 staining of the intercellular clefts. 3D time lapse imaging (1 frame every 15 min for 8 days) revealed the sequential formation of several rosettes (white and blue arrow) in the organoids. **b**. Immunostaining images of the organoids at day 7 (actin (gold), DAPI (blue), Pax6 (magenta) and Sox 2 (green)) could be overlayed with the last image of the live imaging (5 min before fixation) by manual registration of the focus offset. It revealed the presence of $Pax6^{+}$ cells exclusively around the older rosettes (white arrow). **c.** Representative time lapse imaging of live neuroectoderm (lifeact GFP) (N=100) imaged sequentially in 3D (70 optical sections separated by 1 µm), every 15 minutes during 125 hours (spread over 8 consecutive days). The rosettes were manually tracked (red contour) from the day of induction (day 2). Schematic of the peeling of the Jewell chip and collection of the organoids after 3D live monitoring to enable mRNA extraction. RT-qPCR performed on 11 genes, demonstrating the expected reduction in pluripotent reporters (green) and the increase of the neuroectoderm markers (blue) (N=3 replicates, > 1000 organoids/replicate). P-values: ****<0.0001, ***<0.001, **<0.01, *<0.05, ns: non-significative.

.